Hindawi Publishing Corporation
Journal of Nanomaterials
Volume 2015, Article ID 940985, 10 pages
http://dx.doi.org/10.1155/2015/940985

*Research Article*

# $Fe_3O_4$ Nanoparticles Embedded Sodium Alginate/PVP/Calcium Gel Composite for Removal of $Cd^{2+}$

**Long Jiao,[1,2] Peishi Qi,[1,2] Yunzhi Liu,[1,2] Bo Wang,[1,2] and Lili Shan[1,2]**

[1]*State Key Laboratory of Urban Water Resource and Environment, Harbin Institute of Technology, Harbin 150090, China*
[2]*School of Municipal and Environmental Engineering, Harbin Institute of Technology, Harbin 150090, China*

Correspondence should be addressed to Peishi Qi; qipeishi@163.com

Received 26 January 2015; Revised 19 April 2015; Accepted 26 April 2015

Academic Editor: Mohammad S. Akhatar



Magnetic ferroferric oxide ($Fe_3O_4$) nanoparticles embedded sodium alginate (SA)/polyvinylpyrrolidone (PVP)/calciumgel composites (MSPC) were synthesized for the removal of $Cd^{2+}$. The physicochemical properties of the composite gel ball were characterized by scanning electron microscopy (SEM), energy-dispersive X-ray spectroscopy (EDX), power X-ray diffraction patterns (XRD), and vibrating sample magnetometer (VSM). Quantitative adsorptions experiments were performed in view of sorbent dosage, pH, contact time, and temperature. Results showed that the optimum quantity of particles was 1.2 $g{\cdot}L^{-1}$, when the $Cd^{2+}$ concentration was fixed at 150 mg/L. The optimum pH for adsorption is 6.2. When the initial $Cd^{2+}$ concentration was from 50 to 200 $mg{\cdot}L^{-1}$, the adsorption equilibrium time was 80–120 minutes. The isotherms results showed the maximum sorption was 97.8 mg/g calculated from the Langmuir isotherm. The pseudo-second-order kinetic model could be well described by the sorption of $Cd^{2+}$ in the sediment. The correlation coefficients ($R^2$) were all higher than 0.96. Results showed that MSPC was a practical and low-cost material for heavy metal removal from the river sediment and simultaneously solves the problems in convenient separation under additional magnetic field.

## 1. Introduction

Nowadays, river sediment contamination by heavy metals has become an important problem for environmental considerations. Emission of the wastewater effluents containing heavy metal ions has significantly toxic influence on human beings and ecological systems [1, 2]. The heavy metal ions were deposited in river sediment and then released with the change of the surrounding environmental conditions. The situ and ex situ remediation are traditional improvement for heavy metal pollution. These two methods are based on physical, chemical, and biological treatments in the process of ecological restoration.

In the traditional remediation, conventional chemical methods contain extraction and filtration [3], redox, fixed adsorption, ion exchange, and electrodialysis [4]. Among these methods, fixed adsorbent has been accepted for the removal of low content of heavy metals ions [5]. Numerous adsorbents, such as activated carbon, minerals, calcium nitrate, resins, and aluminum hydroxide, were available for heavy metal removal and recovery. Adsorbents can efficiently decrease the content of heavy metals complexed by fixed site. Some of these methods can obtain good separation efficiency for contaminated sediment when metal ions are at high concentration levels. Magnetic techniques and materials using $Fe_3O_4$ nanoparticles for the removal of heavy metals have been reported [6, 7]. $Fe_3O_4$ particles that possess superparamagnetic feature [8], convenient separation characteristics, and independent recycling properties under a magnetic field have been increasingly used in the fields of bioscience and medicine [9, 10]. Therefore, immobilization of $Fe_3O_4$ into some biological polymer materials seems to be a promising alternative [11].

As a kind of natural polysaccharide, sodium alginate (SA) has the stability, solubility, viscosity, and security properties. Its unique biocompatibility, biodegradability, immunogenicity, nontoxicity, and abundant carboxyl groups in the network make alginate beads an effective candidate for pollutant removal [12, 13]. The synthesis of alginate-goethite beads and the application in Cr(VI) and Cr(III) removal have been

Table 1: The concentration of metal ions from the river sediment.

| Sediment | Cd | As | Cr | Cu | Pb | Ni |
|---|---|---|---|---|---|---|
| Sample 1 | 0.125 | — | 0.723 | 0.307 | 0.916 | 0.382 |
| Sample 2 | 0.036 | — | 1.096 | 0.632 | 0.41 | 0.556 |
| Sample 3 | 0.034 | — | 1.079 | 0.614 | 0.415 | 0.561 |

reported [14, 15]. Immobilization of $Fe_3O_4$ nanoparticles into polymeric biomaterials, especially by using polysaccharide and crosslinking agent, was studied [16].

Immobilization of magnetic $Fe_3O_4$ nanoparticles within biological materials, such as agar, agarose, chitosan, collagen, and calcium [17, 18], is an essential step for industrial scale-up of biomass sorption by providing adequate size, density, and mechanical strength required by continuous systems [19]. Alginate can form a reticulated structure when it contacts with calcium and polymer, and then it has been used to immobilize activated carbon and metal hydroxides for removal of organic compounds [20].

This work aims to immobilize magnetic $Fe_3O_4$ nanoparticles into sodium alginate (SA)/polyvinylpyrrolidone (PVP)/calcium gel composite (MSPC) for removal of $Cd^{2+}$ in the river sediment. The MSPC was characterized using scanning electron microscopy (SEM), energy-dispersive X-ray spectroscopy (EDX), X-ray diffraction patterns (XRD), and vibrating sample magnetometer (VSM). The effects of pH and contact time on adsorption capacity were tested, and the isotherms and kinetics data were obtained by the experiment.

## 2. Materials and Methods

*2.1. Materials and Instruments.* Sodium alginate (biochemical grade) and polyvinylpyrrolidone (a molecular weight of ca. 1,300,000, chemical grade) were purchased from Sinopharm Chemical Reagent Co. Ltd, China. Magnetic $Fe_3O_4$ nanoparticles were prepared according to the reported procedure [21]. Calcium nitrate anhydrous ($CaNO_3$) was served as the cross-linker for PVP and SA. Cadmium acetate dihydrate ($C_4H_6CdO_4{\cdot}2H_2O$) and ammonium hydroxide ($NH_3{\cdot}H_2O$) were from Aladdin Co. Ltd. All purchased chemicals were received without any purification.

The sediment was obtained from Songhua River by heavy metals pollution in Harbin China. In this study, the objective of main heavy metal was $Cd^{2+}$. So cadmium acetate dihydrate ($C_4H_6CdO_4{\cdot}2H_2O$) was added to the river sediment in order to reach different experiment concentrations of $Cd^{2+}$ ions. As listed in Table 1, other metal ions content was so low that cannot affect the overall removal efficiency.

Scanning electron microscopy (SEM, HITACHI S-4800) was employed to analyze the surface morphologies of the products and the elemental composition. Energy-dispersive X-ray spectroscopy (EDX, Quanta-200, USA) was used to characterize the samples after gold plating at an accelerating voltage of 20 kV. X-ray diffraction patterns (XRD, D/Max-2550pc, Rigaku inc., Japan) were used with Cu-K$\alpha$radiation ($\lambda$ = 0.1542 nm). The magnetic properties were assessed with VSM (JDM-14D, Jilin University, China). All the wastewater and sediment parameters were determined by inductively coupled plasma mass spectrometry (ICP-MS, Thermo Electron X Series II ICP apparatus).

*2.2. Preparation of Sorbent.* Adsorption of particles preparation process is performed as follows.

2 g SA (dry weight) was dissolved in 100 mL water and 0.5 g PVP was added to the sodium alginate solution and stirred for 0.5 h at 25°C. Then the magnetic $Fe_3O_4$ particles were added into SA/PVP mixture and stirred until completely mixed. Subsequently, the blended mixture was added to 20 mL $Ca(NO_3)_2$ (20 g/L) and dried in a vacuum oven for 24 h at 60°C. Finally, MSPC was obtained and stored at a sealed bottle for further use, and preparation of sodium alginate/PVP/calcium gel composite (SPC) was same to MSPC except for adding $Fe_3O_4$ particles.

*2.3. Adsorption Experiments.* All the following adsorption experiments were performed by a batch method in which the experimental conditions, the ratio of the mud mixture containing $Cd^{2+}$, and MSPC were prepared according to their different needs.

The influence of pH ranging from 1 to 7.5 was examined. The pH values of the solutions were adjusted by 0.1 M HCl or 0.1 M NaOH. The optimized pH for the adsorption derived from the experimental results was adopted for all the experiments. Adsorption kinetics and the effect of contact time were investigated at three temperatures (293 K, 303 K, and 313 K). The MSPC were put into 100 mL of $Cd^{2+}$ solution (50–200 mg/L) at 293 K at pH value of 6.2, and the concentration of $Cd^{2+}$ in the solution was detected at fixed time.

MSPC adsorption capacity $Q_e$ and pollutant removal rate $R$(%) were calculated by the following formula:

$$Q_e = \frac{(C_0 - C_e)V}{W},$$
$$R\,(\%) = \frac{C_0 - C_e}{C_0} \times 100\%, \tag{1}$$

where $C_0$ (mg/L) is the initial concentration of $Cd^{2+}$, $C_e$ (mg/L) is the concentration of $Cd^{2+}$ at equilibrium, $W$ (g) is the mass of the adsorbent (dry), and $V$ (L) is the volume of the solution.

## 3. Results and Discussion

*3.1. Particle Size and Structure of the MSPC.* Figure 1 shows the photographs of MSPC. Immobilization of $Fe_3O_4$ particles made MSPC gel ball partly black in Figure 1(a). The size of the synthesized gel balls is asymmetric with a mean diameter of 4.0 mm. Figure 1(b) shows the MSPC gel balls were absorbed by the super magnet. And the MSPC gel balls were agglomerate material synthesized by immobilization. After that, the MSPC gel balls were put into the sediment in Figures 1(c) and 1(d).

The SEM images of the inner structure of the SPC and MSPC are given in Figures 2(a) and 2(b), respectively. As shown in Figure 2(a), the sodium alginate surface was loose and smooth. Meanwhile, lots of tiny interspace structures

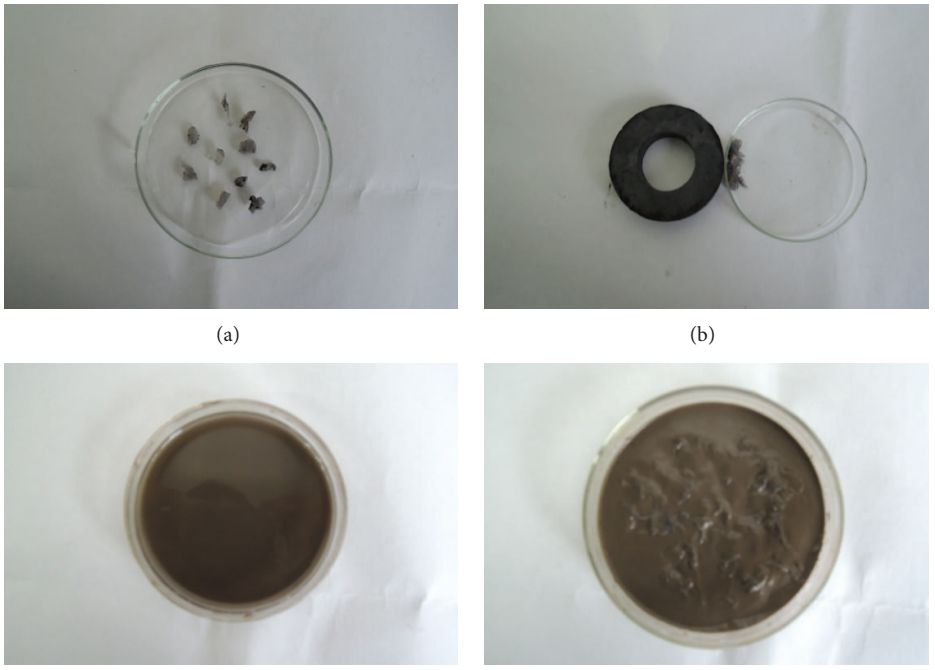

(a) (b)

(c) (d)

Figure 1: Photographs of MSPC (a, b) and photographs of MSPC mixed in the sediment (c, d).

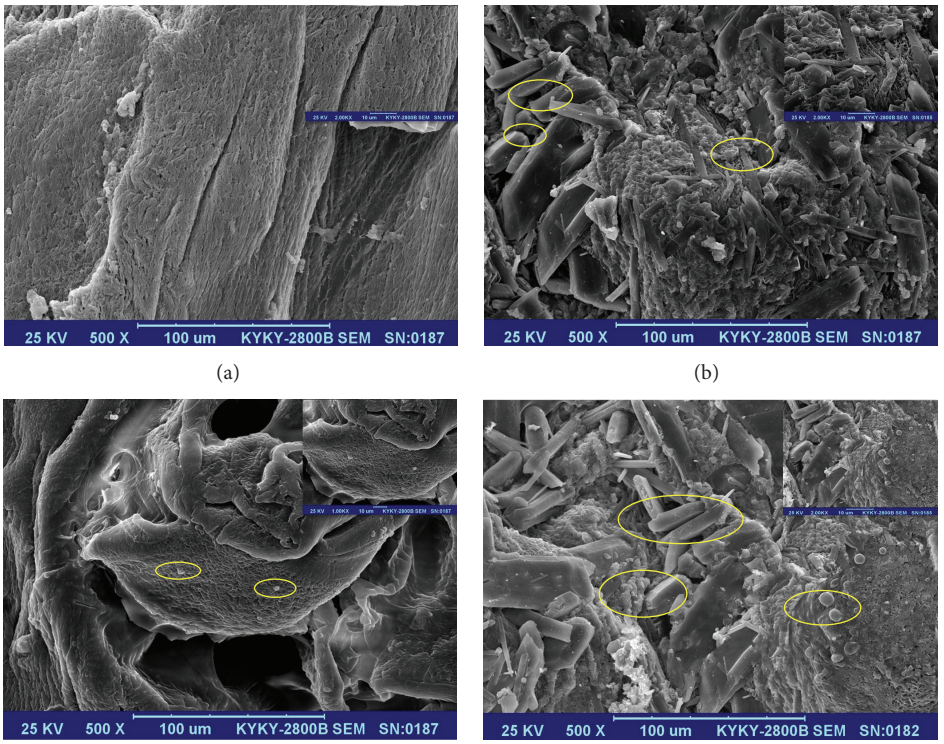


(a) (b)

(c) (d)

Figure 2: SEM image of material surface: SPC (a), MSPC (b), SPC after absorption (c), and MSPC after absorption (d).

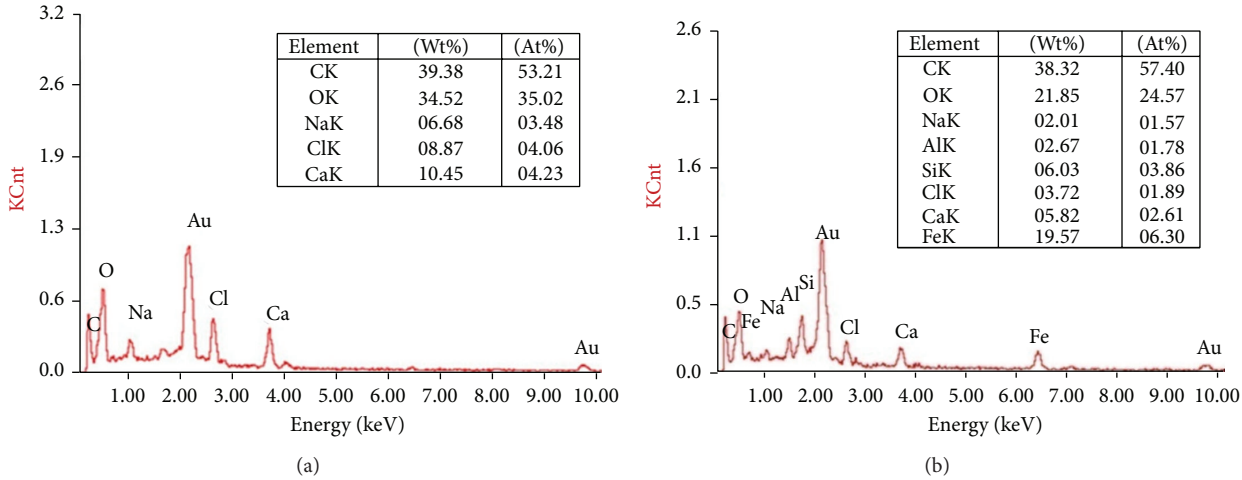


(a) (b)

Figure 3: EDX spectra of the SPC gel balls (a) and the MSPC gel balls (b).

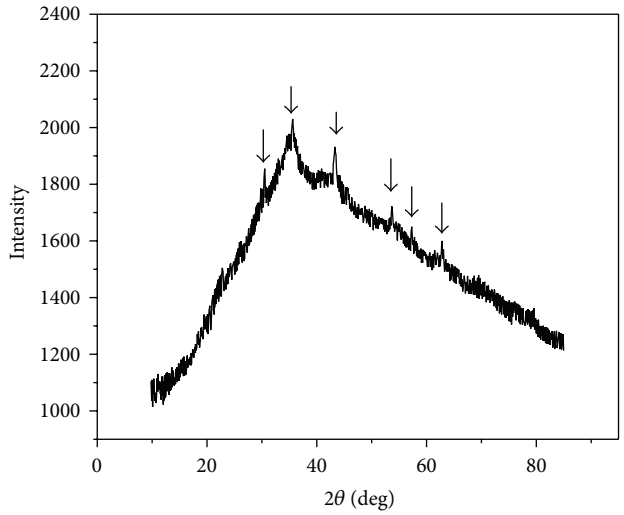


Figure 4: XRD pattern of the MSPC gel balls.

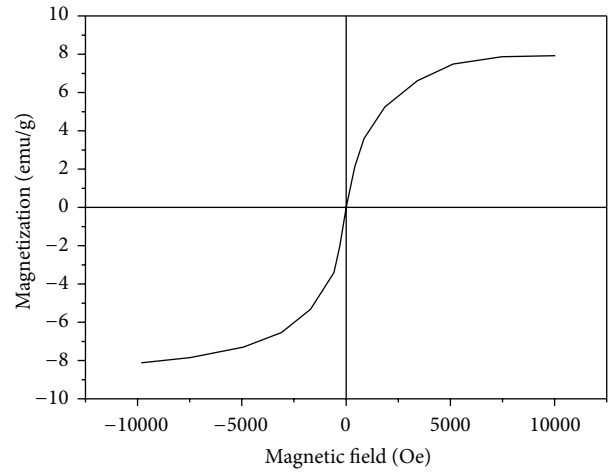


Figure 5: Magnetic hysteresis loop of the MSPC.

can be adsorbed easily by the adsorbents [22]. SEM images in Figure 2(b) show the inner structure of the MSPC where porous microstructure and $Fe_3O_4$ nanoparticles spread over their surface. Figures 2(c) and 2(d) present the SEM image of SPC and MSPC that have absorbed $Cd^{2+}$, the differences are more obvious, and $Fe_3O_4$ nanoparticles are visible on the MSPC surface.

The EDX spectra are given in Figure 3. The signal of Au could be due to the gold plating for measurement. In Figure 3, carbon, oxygen, sodium, chlorine, and calcium elements are detected for SPC, which are the basic components of SPC, while for MSPC, a large amount of iron element has been detected, confirming that $Fe_3O_4$ was on the adsorbent surface and had been embedded by sodium alginate and PVP. And there are small amounts of aluminum and silicon in the $Fe_3O_4$. The presence of these elements does not affect the adsorbent. Thus, a kind of adsorption characteristic composite has been achieved in this work.

*3.2. XRD Analysis.* Figure 4 showed the XRD pattern of MSPC. Six characteristic peaks at 30.5(220), 35.6(311), 43.3(400), 53.7(422), 57.3(511), and 62.8(440) were corresponded well to the planes of spinel structured $Fe_3O_4$. However, the intensities were much lower than those of peaks in the database, which could be explained by the cross-link reaction between $Fe_3O_4$ and the sodium alginate, while the reaction process did not give rise to the phase change of $Fe_3O_4$, which was well consistent with the literature [20].

*3.3. Magnetism Analysis.* Magnetic properties of MSPC were characterized by measuring the hysteresis and remanence curves, as shown in Figure 5. The shape of the magnetization curves was smooth and parabolic, and the saturation magnetization (Ms) was measured to be 7.92 emu/g. The MSPC exhibited nearly super-paramagnetic properties. It indicated the MSPC was characteristic of magnetic response under the added magnetic field, which made it easy to remove metal ions absorbed by the MSPC.

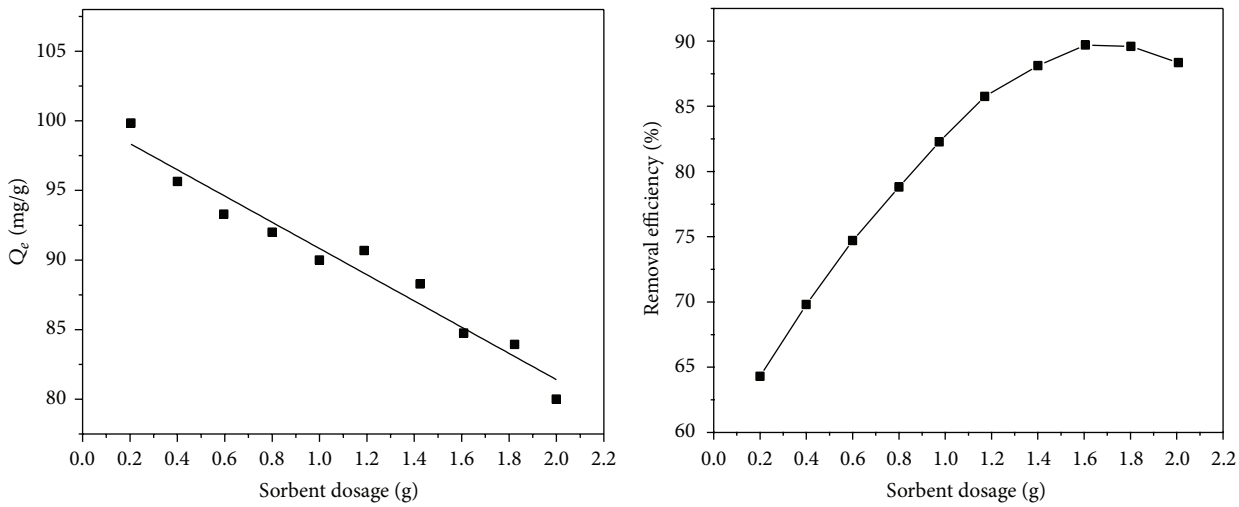


Figure 6: Effect of sorbent dosage on the $Q_e$ (a) and sorbent dosage on the removal efficiency of $Cd^{2+}$ (b).

Table 2: Adsorption isotherm parameters of MSPC gel balls for $Cd^{2+}$.

| $T$ (K) | Langmuir | | | Freundlich | | | D-R isotherm | | |
|---|---|---|---|---|---|---|---|---|---|
| | $Q_m$ (mg/g) | $B$ (L/mg) | $R^2$ | $K_f$ | $1/n$ | $R^2$ | $Q_m$ (mg/g) | $E$ (kJ/mol) | $R^2$ |
| 293 | 97.8 | 0.28 | 0.984 | 20.13 | 1.25 | 0.702 | 98.7 | 14.35 | 0.960 |
| 303 | 94.3 | 0.19 | 0.953 | 19.36 | 1.11 | 0.404 | 92.8 | 13.22 | 0.809 |
| 313 | 84.4 | 0.12 | 0.964 | 13.41 | 1.02 | 0.882 | 86.2 | 9.98 | 0.989 |

*3.4. Effect of Sorbent Dosage.* The adsorption capacity of MSPC and the removal rate of $Cd^{2+}$ could be affected by the sorbent dosage. Figure 6 shows the effect of MSPC dosage ranging from 0.2 g to 2.0 g on adsorption capacity. The concentration $Cd^{2+}$ of 150 mg/L could be representative of the high levels pollution of heavy metals in the river sediment. As shown in Figure 6, the removal rate of $Cd^{2+}$ increases with the concentration of MSPC. However, the adsorption capacity of MSPC is close to the saturation at the same situations. Keeping $Cd^{2+}$ concentration of 150 mg/L, adsorbent adsorption capacity changes a little at the range of 80–100 mg/g. It showed that adapted holding MSPC mass content was positive for $Cd^{2+}$ removal. As seen from Figure 6(b), the optimal quantity of particles is 1.2 g/L, in which the removal efficiency of $Cd^{2+}$ (100 mL, 150 mg/L) in the river sediment is about 87%.

*3.5. Effect of pH Value.* pH value, which affects the formation distribution of heavy metals in sediment solution by influencing the other components of sediment the same time, also indirectly affects the removal efficiency of the heavy metals. The effect of pH on the adsorption properties is shown in Figure 7. Clearly, the adsorption capacity was enhanced quickly with pH increase from 1 to 2 but slowly with pH from 2 to 6. At pH value of 6.2, maximum adsorption quantity is obtained. When the pH value exceeds 7, the uptake decreases because the cadmium ions start to precipitate as $Cd(OH)_2$, which is also a kind of sediment. At lower pH values, the functional groups for coordination including $H^+$ and $Cd^{2+}$ groups compete for adsorption sites, which do not favor the adsorption. When the solution pH values is increased, the competitive adsorption is reduced, so more negatively charged adsorption sites can positively charge the $Cd^{2+}$.

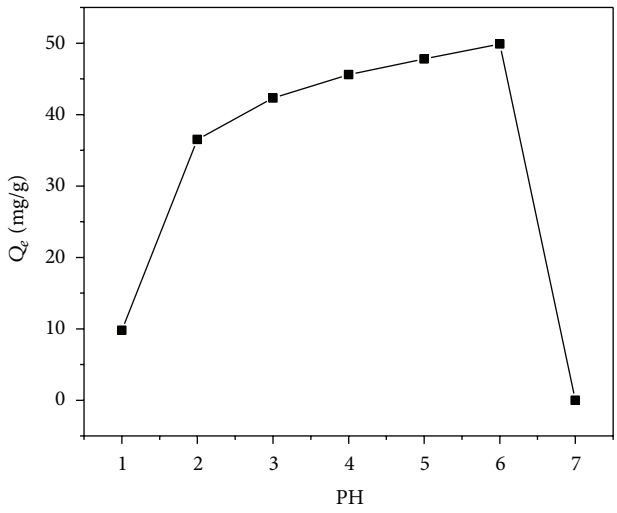


Figure 7: Effect of pH value on the adsorption of $Cd^{2+}$ by MSPC.

*3.6. Effect of Contact Time.* The effect of contact time on the adsorption process is shown in Figure 8. With the increase

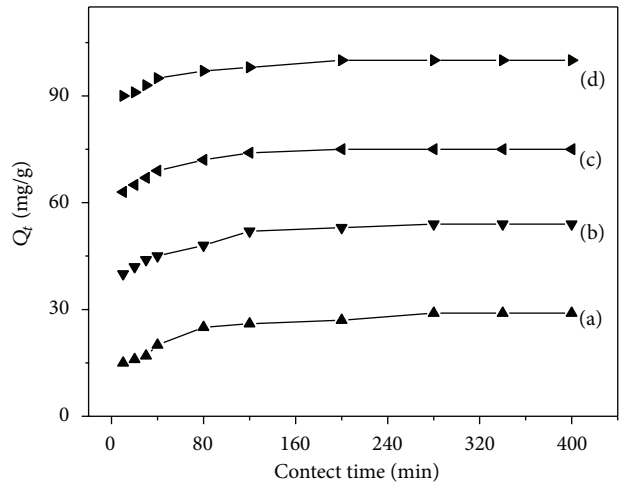


FIGURE 8: Effect of contact time on the adsorption of $Cd^{2+}$ by MSPC.

of contact time, the adsorption of volume cadmium ions is increased. When the adsorption time is 120 min, adsorption capacity reaches the maximum. When the initial concentration of $Cd^{2+}$ is 50 and 100 mg/L, adsorption equilibrium time is 80–90 min. SA and $Fe_3O_4$ nanoparticles form a mesh with granular structure through the macromolecular cross-linking together. The initial concentration of $Cd^{2+}$ is changed to 150 and 200 mg/L, and adsorption equilibrium time is 90–120 min. When the active sites are limited, more competition $Cd^{2+}$ ions limit combining site resulted in the added adsorption equilibrium time. Therefore, the MSPC with open structure and three-dimensional polymer network reinforce $Cd^{2+}$ adsorption into active sites, which could increase the adsorption rate and adsorption capacity.

*3.7. Sorption Isotherms.* Langmuir, Freundlich, and D-R isotherm models were employed for adsorption data correlation to quantify the adsorption capacity of MSPC in Figure 9. The linear forms of these three models are listed as follows [23, 24]:

$$\begin{aligned}
\text{Langmuir model: } & \frac{C_e}{Q_e} = \frac{1}{BQ_m} + \frac{C_e}{Q_m}, \\
\text{Freundlich model: } & \ln Q_e = \ln K_f + \frac{1}{n} \ln C_e, \\
\text{D-R model: } & \ln Q_e = \ln Q_m + K\varepsilon^2, \\
& \varepsilon = RT \ln\left(1 + \ln C_e\right), \\
& E = \frac{1}{\sqrt{2K}},
\end{aligned} \tag{2}$$

where $Q_e$ (mg/g) is the amount of adsorbed $Cd^{2+}$ at equilibrium and $C_e$ (mg/L) is the concentration of $Cd^{2+}$ at equilibrium. $K_f$ and $n$ are associated with the adsorption capacity and adsorption intensity, respectively. $B$ (L/mg) is the Langmuir constants. $\varepsilon$ is polanyi potential; $E$ (kJ/mol) is the mean free energy of adsorption.

As listed in Table 2, because of the relatively high correlation parameters, the experimental data can be well described by the three models, in which the Langmuir model gives the best fit ($R^2 > 0.96$). Freundlich parameter, the $K_f$ value, supports the order of cadmium uptake that is 293 K > 303 K > 313 K, which was confirmed by the corresponding $1/n$ values. Langmuir isotherm model is based on the assumption that the dynamic adsorption-desorption processes occur on homogeneous surface, taking no account of the interaction between the MSPC and the solute in Figure 9(a). The maximum sorption calculated from the Langmuir isotherm is 97.8 mg/g. It is slightly greater than the experimental values regarding that there are still unoccupied sorption sites. Obviously, plots of $\ln Q_e$ versus $\ln C_e$ yield a straight line of slope $1/n$ and intercept $\ln K_f$ [25]. The plot isotherm fit is shown in Figure 9(b). The adsorption mechanism of $Cd^{2+}$ is predicted by D-R isotherm model in Figure 9(c). $E$ values relating to the mean free energy of adsorption are 14.35 kJ/mol, 13.22 kJ/mol, and 9.98 kJ/mol at 293 K, 303 K, and 313 K, respectively, which is indicative of the ion-exchange adsorption.

*3.8. Adsorption Kinetics.* In order to reveal the adsorption mechanism, the kinetic data under these three systems are fitted to pseudo-first-order equation, pseudo-second-order equation, and intraparticular diffusion model in Figure 10. The linear form of these three models can be written as follows [26]:

$$\begin{aligned}
\text{First-order equation: } & \ln\left(Q_e - Q_t\right) = \ln Q_e - K_1 t, \\
\text{Second-order equation: } & \frac{t}{Q_t} = \frac{1}{k_2 {Q_e}^2} + \frac{t}{Q_e}, \\
\text{Intraparticular diffusion model: } & Q_t = k_{id} t^{1/2},
\end{aligned} \tag{3}$$

where $Q_e$ and $Q_t$ are the amounts of adsorbed $Cd^{2+}$ (mg/cm$^2$) at equilibrium and at time $t$, respectively. $k_1$ (min$^{-1}$), $k_2$ (g/(mg min)), and $k_{id}$ (mg/(g min$^{1/2}$)) are the rate constants.

The parameters of the three models are summarized in Table 3. Because of low correlation coefficient, first-order reaction kinetics model is not enough to describe $Cd^{2+}$ adsorption on MSPC. The correlation coefficient ($R^2 > 0.96$) indicates that pseudo-second-order model could be representative of the reaction mechanism, pointing to a chemical sorption character in Figure 10(b). SA provide plenty of carboxylic acid and hydroxyl sites, and $Fe_3O_4$ provides surface hydroxyl group, which can be used as active absorption sites with $Cd^{2+}$ ion exchange.

The initial adsorption rate increases with the increase of initial concentration of $Cd^{2+}$. However, when concentration of $Cd^{2+}$ is increased greatly, the initial adsorption rate drops, and the pseudo-second-order model reaction rate constant $K_2$ also shows the same trend. This phenomenon is attributed to the low initial concentration of metal and the abundant adsorption sites of MSPC. But after the initial metal concentration is increased to a certain value, the adsorption quantity reached the saturation, which reveals that most of the active adsorption sites on the adsorbent have been dominated by metal ions [27].

Table 3: Adsorption kinetic parameters of MSPC gel balls for $Cd^{2+}$.

| | Pseudo-first-order | | | Pseudo-second-order | | | Intraparticular diffusion model | | | |
|---|---|---|---|---|---|---|---|---|---|---|
| $C$ (mg/L) | $K_1 \cdot 10^{-2}$ (g/mg min$^{-1}$) | $Q_e$ (mg/g) | $R^2$ | $K_2 \cdot 10^{-2}$ (g/mg min$^{-1}$) | $Q_e$ (mg/g) | $R^2$ | $K_1 d$ (mg/g min$^{1/2}$) | $R^2$ | $K_2 d$ (mg/g min$^{1/2}$) | $R^2$ |
| 50 | 2.37 | 13.22 | 0.895 | 4.95 | 26.73 | 0.986 | 1.46 | 0.983 | 0.03 | |
| 100 | 3.11 | 17.82 | 0.872 | 3.03 | 53.16 | 0.969 | 1.45 | 0.974 | 0.08 | |
| 150 | 2.15 | 24.31 | 0.978 | 1.93 | 78.88 | 0.976 | 2.72 | 0.987 | 0.12 | 0.979 |
| 200 | 1.74 | 32.85 | 0.954 | 1.07 | 108.41 | 0.979 | 3.60 | 0.987 | 0.2 | 0.986 |

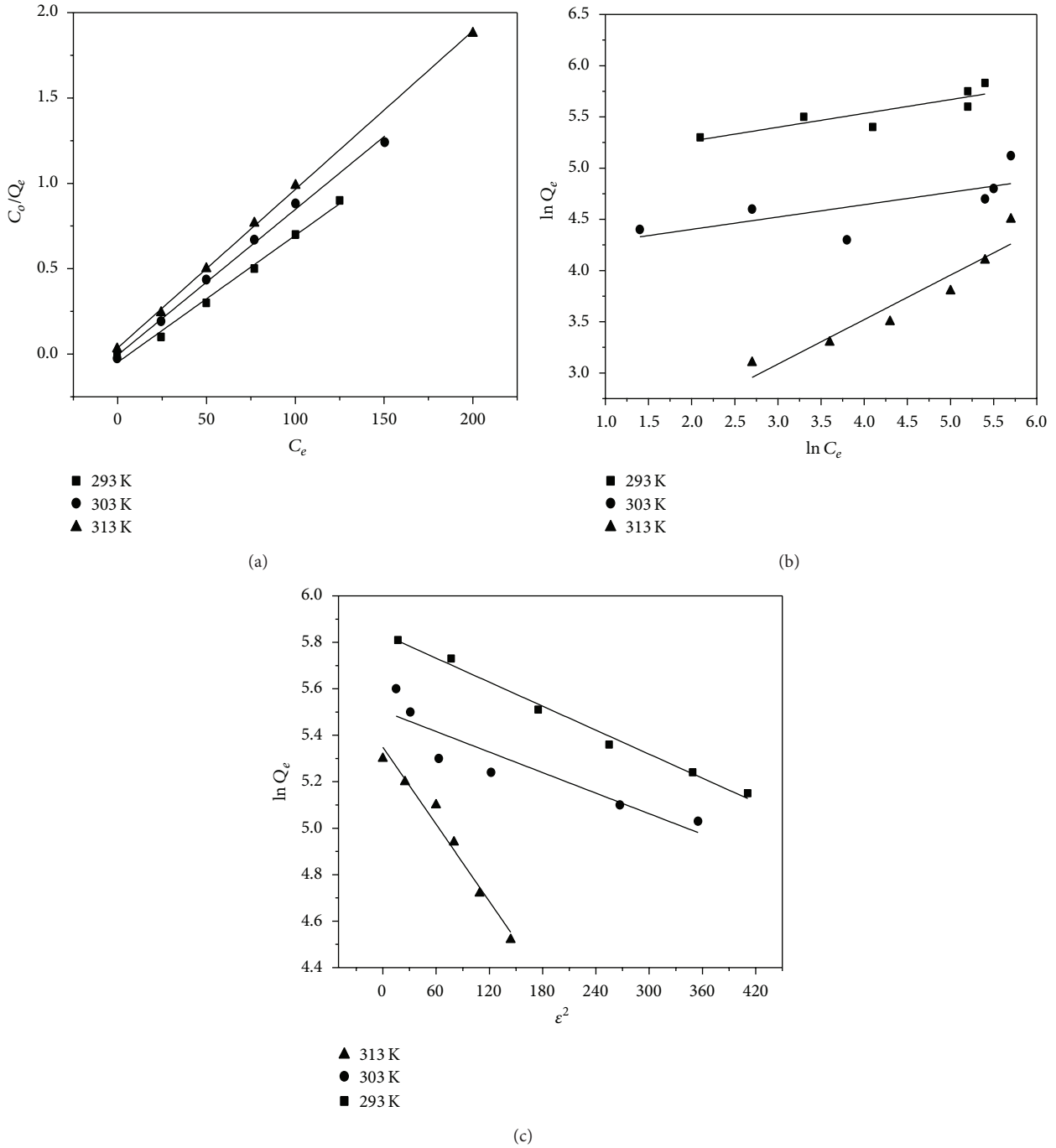


Figure 9: Sorption isotherms fit of $Cd^{2+}$: Langmuir isotherm fit (a), Freundlich isotherm fit (b), and D-R isotherm fit (c).

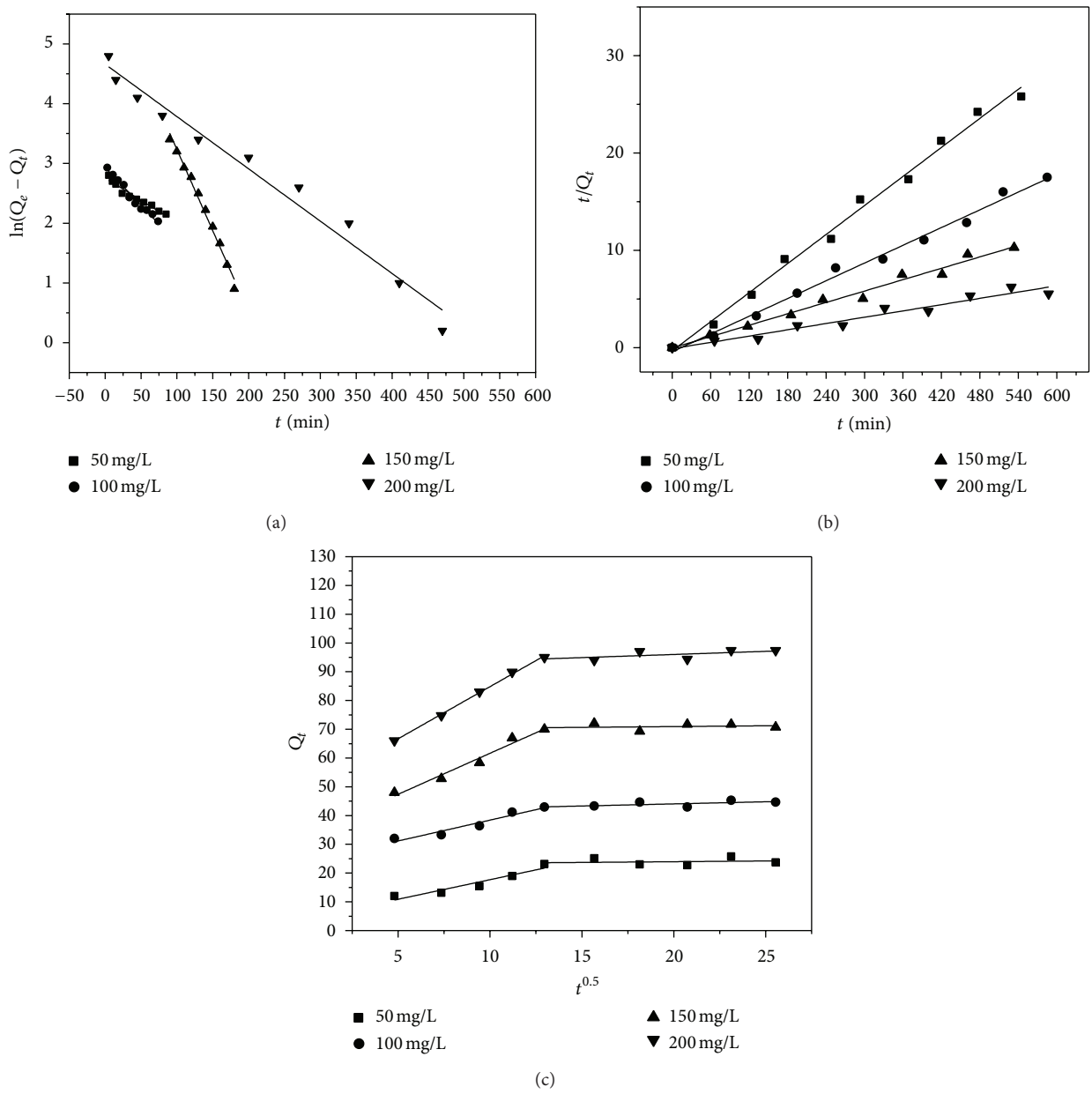


Figure 10: Adsorption kinetics fit of $Cd^{2+}$: pseudo-first-order kinetic fit (a), pseudo-second-order kinetic fit (b), and intraparticular diffusion fit (c).

Intraparticular diffusion is more linear, indicating that intraparticular diffusion is not the limiting step. Adsorption process of $Cd^{2+}$ is the combination of surface adsorption point and spreading reticulated structure inside the tunnel, and the process of joint surface adsorption and intraparticular diffusion control. Intraparticular diffusion equation, which can identify the diffusion mechanism, confirms that two stages occur as mentioned above. When the initial concentration of $Cd^{2+}$ is from 50 to 200 mg/L, $K_{1d}$ is from 1.46 to 3.60 mg/g $min^{1/2}$. The rapid stage is due to MSPC diffusion where the intraparticular diffusion is the rate-limiting step. Comparatively, the slow stage is the equilibrium step where intraparticular diffusion starts to slow down.

## 4. Conclusions

The MSPC were synthesized under different mass fraction of $Fe_3O_4$ nanoparticles, SA and PVP, subsequently treated by immobilization, and finally used for removal of $Cd^{2+}$ from river sediment. Thus, this new adsorbent not only possesses the high adsorption capacity but also is easy to separate from the mud mixture. The conclusions are shown below.

(1) The character analyses indicated that the MSPC had a diameter of about 4 mm, with many tiny interspace structures on the surface and contained amide and hydroxide groups which could absorb metal ions.

(2) SEM elucidated that magnetic $Fe_3O_4$ nanoparticles were embedded successfully and might be distributed asymmetrically. The spinel structure of $Fe_3O_4$ did not change during the synthesized process. The MSPC show 7.92 emu/g Ms by VSM.

(3) The optimum pH for adsorption was 6.2 and the contact time required to achieve equilibrium was 80–120 min, when the initial $Cd^{2+}$ concentration varied from 50 to 200 mg/L. The removal rate of $Cd^{2+}$ is 87%, when the concentration of $Cd^{2+}$ was fixed at 150 mg/L.

(4) The Langmuir adsorption isotherm fits well with the adsorption equilibrium data. The maximum sorption calculated from the Langmuir isotherm was 97.8 mg/g for MSPC in sediment. A pseudo-second-order rate mechanism can be used to illustrate the sorption of MSPC. The correlation coefficients were all $R^2 > 0.96$.

## Conflict of Interests

The authors declare that there is no conflict of interests regarding the publication of this paper.

## References


[1] J. O. Nriagu and J. M. Pacyna, "Quantitative assessment of worldwide contamination of air, water and soils by trace metals," *Nature*, vol. 333, no. 6169, pp. 134–139, 1988.

[2] K. E. Giller, E. Witter, and S. P. Mcgrath, "Toxicity of heavy metals to microorganisms and microbial processes in agricultural soils: a review," *Soil Biology and Biochemistry*, vol. 30, no. 10-11, pp. 1389–1414, 1998.

[3] J. Aguado, J. M. Arsuaga, A. Arencibia, M. Lindo, and V. Gascón, "Aqueous heavy metals removal by adsorption on amine-functionalized mesoporous silica," *Journal of Hazardous Materials*, vol. 163, no. 1, pp. 213–221, 2009.

[4] P. G. Priya, C. A. Basha, V. Ramamurthi, and S. N. Begum, "Recovery and reuse of Ni(II) from rinse water of electroplating industries," *Journal of Hazardous Materials*, vol. 163, no. 2-3, pp. 899–909, 2009.

[5] A. Heidari, H. Younesi, and Z. Mehraban, "Removal of Ni(II), Cd(II), and Pb(II) from a ternary aqueous solution by amino functionalized mesoporous and nano mesoporous silica," *Chemical Engineering Journal*, vol. 153, no. 1–3, pp. 70–79, 2009.

[6] S. M. Ponder, J. G. Darab, and T. E. Mallouk, "Remediation of Cr(VI) and Pb(II) aqueous solutions using supported, nanoscale zero-valent iron," *Environmental Science and Technology*, vol. 34, no. 12, pp. 2564–2569, 2000.

[7] S. A. Kim, S. Kamala-Kannan, K.-J. Lee et al., "Removal of Pb(II) from aqueous solution by a zeolite-nanoscale zero-valent iron composite," *Chemical Engineering Journal*, vol. 217, pp. 54–60, 2013.

[8] Y. S. Kang, S. Risbud, J. F. Rabolt, and P. Stroeve, "Synthesis and characterization of nanometer-size $Fe_3O_4$ and $\gamma$-$Fe_2O_3$ particles," *Chemistry of Materials*, vol. 8, no. 9, pp. 2209–2211, 1996.

[9] C. R. Keenan, R. Goth-Goldstein, D. Lucas, and D. L. Sedlak, "Oxidative stress induced by zero-valent iron nanoparticles and Fe(II) in human bronchial epithelial cells," *Environmental Science and Technology*, vol. 43, no. 12, pp. 4555–4560, 2009.

[10] A. Nacev, C. Beni, O. Bruno, and B. Shapiro, "The behaviors of ferromagnetic nano-particles in and around blood vessels under applied magnetic fields," *Journal of Magnetism and Magnetic Materials*, vol. 323, no. 6, pp. 651–668, 2011.

[11] R. A. Crane and T. B. Scott, "Nanoscale zero-valent iron: future prospects for an emerging water treatment technology," *Journal of Hazardous Materials*, vol. 211-212, pp. 112–125, 2012.

[12] N. A. M. Zain, M. S. Suhaimi, and A. Idris, "Development and modification of PVA-alginate as a suitable immobilization matrix," *Process Biochemistry*, vol. 46, no. 11, pp. 2122–2129, 2011.

[13] Y. Nishio, A. Yamada, K. Ezaki, Y. Miyashita, H. Furukawa, and K. Horie, "Preparation and magnetometric characterization of iron oxide-containing alginate/poly(vinyl alcohol) networks," *Polymer*, vol. 45, no. 21, pp. 7129–7136, 2004.

[14] N. K. Lazaridis and C. Charalambous, "Sorptive removal of trivalent and hexavalent chromium from binary aqueous solutions by composite alginate-goethite beads," *Water Research*, vol. 39, no. 18, pp. 4385–4396, 2005.

[15] J. H. Chen, G. P. Li, Q. L. Liu, J. C. Ni, W. B. Wu, and J. M. Lin, "Cr(III) ionic imprinted polyvinyl alcohol/sodium alginate (PVA/SA) porous composite membranes for selective adsorption of Cr(III) ions," *Chemical Engineering Journal*, vol. 165, no. 2, pp. 465–473, 2010.

[16] X. S. Lv, G. M. Jiang, X. Xue et al., "$Fe^0$-$Fe_3O_4$ nanocomposites embedded polyvinyl alcohol/sodium alginate beads for chromium (VI) removal," *Journal of Hazardous Materials*, vol. 262, pp. 748–758, 2013.

[17] M. Kobaslija and D. T. McQuade, "Removable colored coatings based on calcium alginate hydrogels," *Biomacromolecules*, vol. 7, no. 8, pp. 2357–2361, 2006.

[18] G. I. Olivas and G. V. Barbosa-Cánovas, "Alginate-calcium films: water vapor permeability and mechanical properties as affected by plasticizer and relative humidity," *LWT-Food Science and Technology*, vol. 41, no. 2, pp. 359–366, 2008.

[19] S. Hua, H. Ma, X. Li, H. Yang, and A. Wang, "pH-sensitive sodium alginate/poly(vinyl alcohol) hydrogel beads prepared by combined $Ca^{2+}$ crosslinking and freeze-thawing cycles for controlled release of diclofenac sodium," *International Journal of Biological Macromolecules*, vol. 46, no. 5, pp. 517–523, 2010.

[20] Y.-B. Lin, B. Fugetsu, N. Terui, and S. Tanaka, "Removal of organic compounds by alginate gel beads with entrapped activated carbon," *Journal of Hazardous Materials*, vol. 120, no. 1–3, pp. 237–241, 2005.

[21] Y. Ren, Q. Dong, J. Feng, J. Ma, Q. Wen, and M. Zhang, "Magnetic porous ferrospinel $NiFe_2O_4$: a novel ozonation catalyst with strong catalytic property for degradation of di-n-butyl phthalate and convenient separation from water," *Journal of Colloid and Interface Science*, vol. 382, no. 1, pp. 90–96, 2012.

[22] X. Lv, J. Xu, G. Jiang, J. Tang, and X. Xu, "Highly active nanoscale zero-valent iron (nZVI)-$Fe_3O_4$ nanocomposites for the removal of chromium(VI) from aqueous solutions," *Journal of Colloid and Interface Science*, vol. 369, no. 1, pp. 460–469, 2012.

[23] I. Langmuir, "The adsorption of gases on plane surfaces of glass, mica and platinum," *The Journal of the American Chemical Society*, vol. 40, no. 9, pp. 1361–1403, 1918.

[24] B. P. Bering, M. M. Dubinin, and V. V. Serpinsky, "On thermodynamics of adsorption in micropores," *Journal of Colloid And Interface Science*, vol. 38, no. 1, pp. 185–194, 1972.

[25] H. Freundlich, "Über die absorption in lösungen," *Zeitschrift für Physikalische Chemie*, vol. 57, pp. 385–470, 1906 (German).

[26] W. J. Weber and J. C. Morris, "Kinetics of adsorption on carbon from solution," *Journal of the Sanitary Engineering Division*, vol. 89, no. 2, pp. 31–60, 1963.

[27] J. Yang, M. Yu, and T. Qiu, "Adsorption thermodynamics and kinetics of Cr(VI) on KIP210 resin," *Journal of Industrial and Engineering Chemistry*, vol. 20, no. 2, pp. 480–486, 2014.